Monthly Notices
of the
ROYAL ASTRONOMICAL SOCIETY

MNRAS **450,** 3069–3079 (2015) doi:10.1093/mnras/stv866

The stellar spectral features of nearby galaxies in the near infrared: tracers of thermally pulsing asymptotic giant branch stars?

Rogério Riffel,[1⋆] Rachel E. Mason,[2] Lucimara P. Martins,[3] Alberto Rodríguez-Ardila,[4] Luis C. Ho,[5,6] Rogemar A. Riffel,[7] Paulina Lira,[8] Omaira Gonzalez Martin,[9,10] Daniel Ruschel-Dutra,[1,9] Almudena Alonso-Herrero,[11] Helene Flohic,[12] Richard M. McDermid,[2,13,14] Cristina Ramos Almeida,[9,10] Karun Thanjavur[15] and Claudia Winge[16]

[1]*Departamento de Astronomia, Universidade Federal do Rio Grande do Sul. Av. Bento Gonçalves 9500 Porto Alegre, RS, Brazil*
[2]*Gemini Observatory, Northern Operations Center, 670 N. A'ohoku Place, Hilo, HI 96720, USA*
[3]*NAT – Universidade Cruzeiro do Sul, Rua Galvão Bueno, 868, 01506-000, São Paulo, SP, Brazil*
[4]*Laboratório Nacional de Astrofísica – Rua dos Estados Unidos 154, Bairro das Nações. CEP 37504-364, Itajubá, MG, Brazil*
[5]*Kavli Institute for Astronomy and Astrophysics, Peking University, Beijing 100871, China*
[6]*Department of Astronomy, School of Physics, Peking University, Beijing 100871, China*
[7]*Departamento de Física/CCNE, Universidade Federal de Santa Maria, 97105-900 Santa Maria, RS, Brazil*
[8]*Departamento de Astronomía, Universidad de Chile, Casilla 36-D, Santiago, Chile*
[9]*Instituto de Astrofísica de Canarias, Calle Vía Láctea, s/n, E-38205 La Laguna, Tenerife, Spain*
[10]*Departamento de Astrofísica, Universidad de La Laguna, E-38205 La Laguna, Tenerife, Spain*
[11]*Instituto de Fisica de Cantabria, CSIC-UC, E-39005 Santander, Spain*
[12]*University of the Pacific, Department of Physics, 3601 Pacific Avenue, Stockton, CA 95211, USA*
[13]*Australian Astronomical Observatory, PO Box 296, Epping, NSW 1710, Australia*
[14]*Department of Physics and Astronomy, Macquarie University, NSW 2109, Australia*
[15]*Department of Physics & Astronomy, University of Victoria, Victoria, BC, V8P 1A1, Canada*
[16]*Gemini Observatory, Southern Operations Center, c/o AURA, Casilla 603, La Serena, Chile*

Accepted 2015 April 15. Received 2015 April 15; in original form 2014 December 29

ABSTRACT

We analyse the stellar absorption features in high signal-to-noise ratio (S/N) near-infrared (NIR) spectra of the nuclear region of 12 nearby galaxies, mostly spirals. The features detected in some or all of the galaxies in this sample are the TiO (0.843 and 0.886 μm), VO (1.048 μm), CN (1.1 and 1.4 μm), H_2O (1.4 and 1.9 μm) and CO (1.6 and 2.3 μm) bands. The C_2 (1.17 and 1.76 μm) bands are generally weak or absent, although C_2 (1.76 μm) may be weakly present in the mean galaxy spectrum. A deep feature near 0.93 μm, likely caused by CN, TiO and/or ZrO, is also detected in all objects. Fitting a combination of stellar spectra to the mean spectrum shows that the absorption features are produced by evolved stars: cool giants and supergiant stars in the early- or thermally pulsing asymptotic giant branch (E-AGB or TP-AGB) phases. The high luminosity of TP-AGB stars, and the appearance of VO and ZrO features in the data, suggest that TP-AGB stars dominate these spectral features. However, a contribution from other evolved stars is also likely. Comparison with evolutionary population synthesis models shows that models based on empirical libraries that predict relatively strong NIR features provide a more accurate description of the data. However, none of the models tested accurately reproduces all of the features observed in the spectra. To do so, the models will need to not only improve the treatment of TP-AGB stars, but also include good quality spectra of red giant and E-AGB stars. The uninterrupted wavelength coverage, high S/N and quantity of features we present here will provide a benchmark for the next generation of models aiming to explain and predict the NIR properties of galaxies.

Key words: stars: AGB and post-AGB – galaxies: active – galaxies: bulges – galaxies: stellar content.

⋆ E-mail: riffel@ufrgs.br

1 INTRODUCTION

Studying the unresolved stellar content of galaxies generally involves disentangling the various components contributing to the spectral energy distribution (SED), fitting a combination of simple stellar populations (SSPs) to derive information about age, metallicity and star formation history. In the near-infrared (NIR, 0.85–2.5 μm), the thermally pulsing asymptotic giant branch (TP-AGB) phase – the last stage of the evolution of intermediate-mass stars ($M \lesssim 6$ M⊙) – is a particularly important component of the SSP models. These stars may be able to dominate the emission of stellar populations with ages ∼0.2–2 Gyr (Maraston 2005, see also Mouhcine & Lançon 2002 and Dottori et al. 2005) being responsible for roughly half of the luminosity in the *K* band (Salaris et al. 2014).

Unfortunately, a correct treatment of the TP-AGB phase is difficult to achieve, since the physics of the evolution of this stellar phase is still poorly known (Maraston 2005; Marigo et al. 2008; Conroy & Gunn 2010; Kriek et al. 2010; Conroy 2013; Noël et al. 2013; Zibetti et al. 2013). The complex processes occurring during this phase (mass-loss, changing opacities, dredge-up events, etc.) are difficult to accurately model, and must be anchored with empirical calibrations (e.g. Marigo et al. 2008). The contribution of a population of TP-AGB stars to the light of a galaxy also depends on the duration of this evolutionary stage, which is not yet well constrained. In addition, the features of an observed spectrum of a TP-AGB star depend strongly on its age and metallicity (e.g. Lançon et al. 2001), and we do not have NIR empirical spectra of stars covering the full range of these parameters expected in galaxies.

These difficulties have led to the production of models making very different predictions for the NIR spectral region. In contrast to evolutionary population synthesis (EPS) models based on isochrone synthesis, such as those of Bruzual & Charlot (2003, hereafter BC03), the models of Maraston (2005) and Maraston & Strömbäck (2011, hereafter M05 and M11), based on the fuel consumption theory and using empirical spectra of C- and O-rich stars for the TP-AGB phase, predict the presence of strong NIR molecular features, such as TiO (0.843 μm, 0.886 μm), CN (1.1 μm, 1.4 μm), C_2 (1.17 μm, 1.76 μm), H_2O (1.4 μm, 1.9 μm) and CO (1.6 μm, 2.3 μm) at the ages where these stars are abundant. When applied to galaxy spectra, the M05 models also predict much higher NIR luminosities than the BC03 ones (Maraston et al. 2006). The models are calibrated using Galactic and Magellanic Cloud globular clusters, and have been tested against a variety of astronomical data sets, with somewhat mixed results (Maraston et al. 2006; Kriek et al. 2010; Lyubenova et al. 2010, 2012; Riffel et al. 2011a; Melbourne et al. 2012; Zibetti et al. 2013; Marigo 2014).

Given the challenges involved in constructing SSPs appropriate to modelling galaxy SEDs based solely on theoretical stellar spectra and/or limited empirical stellar spectra, searches for these bands in galaxies would be a valuable step forward in guiding the development and improvement of the models. Some studies have been carried out in this area. The 1.1 μm CN band, for example, has been detected in AGN and starburst galaxies (Riffel et al. 2007; Ramos Almeida, Pérez García & Acosta-Pulido 2009), along with the 1.4 μm CN band in a single object (Martins et al. 2013b). The CO bandheads near 2.3 μm are well known, and the first detection of ZrO features at 0.8–1.0 μm was recently reported in a sample of starburst nuclei (Martins et al. 2013b). Conversely, Zibetti et al. (2013) do not detect the TP-AGB spectral features predicted by M05 in their spectra of post-starburst galaxies at $z \sim 0.2$.

Here we investigate the origin of the stellar molecular absorption features in NIR spectra of 12 nearby galaxies, and use the spectra to test two current EPS models. The detected bands include CN (1.1 μm, 1.4 μm), CO (∼1.6 μm, ∼2.3 μm), H_2O (∼1.4 μm, ∼1.9 μm), VO (1.048 μm) and TiO (0.843 μm, 0.886 μm). We also detect a feature at ∼0.93 μm which is probably due to a blend of CN, TiO and ZrO bands. A tentative detection of a C_2 (1.76 μm) bandhead in the mean spectrum of the whole sample is also reported. While some of these bands have been discussed in previous work, the novelty of this study is the simultaneous detection and analysis of many features over a wide range of wavelengths.

2 SAMPLE AND DATA

2.1 The sample

The galaxies in this paper (Table 1) are a subset of those observed for the Palomar XD project (Mason et al. 2015). That program acquired high-quality nuclear NIR spectra of galaxies in the Palomar survey of nearby galaxies (Ho, Filippenko & Sargent 1995,

Table 1. Galaxy properties.

Galaxy	Distance[a] (Mpc)	Morphology[a]	AGN[a]	log L(H α)[a] (erg s^{-1})	Age (ref)[b]	Aperture[c] (pc)	SNR[d]
NGC 2655	24.4	Sa	S2	39.55	I (1)	27 × 82	118
NGC 2768	23.7	S0/E6	L2	39.01	I (1,2), O (3,4)	27 × 80	121
NGC 2832	91.6	E3	L2	38.91	O (2,5)	135 × 404	160
NGC 3147	40.9	S(s)b I-II	S2	39.47	O (6)	54 × 163	132
NGC 3718	17.0	Sa	L1.9	38.46	–	19 × 58	123
NGC 4548	16.8	SB(sr)b I-II	L2	38.46	O (7)	9 × 28	110
NGC 4565	9.7	Sb	S1.9	37.97	–	24 × 73	100
NGC 4594	20.0	Sab	L2	39.70	O (8)	21 × 63	168
NGC 4750	26.1	S(r)	L1.9	39.04	–	31 × 94	119
NGC 5005	21.3	S(s)b II	L1.9	39.47	I/O (9)	19 × 56	119
NGC 5371	37.8	SB(sr)b I	L2	39.24	–	50 × 149	100
NGC 5850	28.5	SB(rs)b I-II	L2	38.66	O (10)	50 × 149	100

Notes. [a]Ho et al. (1997) and references therein. [b]Stellar population age. O = old, age $\gtrsim$5 Gyr. I = intermediate age, age ∼1–2 Gyr. References: 1 – Sil'chenko (2006). 2 – Zhang et al. (2008) 3 – Serra et al. (2008). 4 – Crocker et al. (2008). 5 – Loubser et al. (2009). 6 – BC03. 7– Sarzi et al. (2005). 8 – Sánchez-Blázquez et al. (2006). 9 – Cid Fernandes et al. (2004b). 10 – de Lorenzo-Cáceres, Falcón-Barroso & Vazdekis (2013) [c]Slit width × extraction aperture of 0.3 arcsec × 0.9 arcsec. [d]Determined in the range 2.076–2.096 μm.

1997), using the Gemini Near-Infrared Spectrograph (GNIRS) on the Gemini North telescope (Elias et al. 2006). The GNIRS sample contains AGNs covering a wide range of luminosity and accretion rate. Of these, a subsample was selected for this study on the basis of high signal-to-noise ratio (S/N) data, strong stellar continuum, weak AGN emission and excellent cancellation of the strong telluric absorption coincident with the location of the CN and H_2O bands around 1.4 μm. While some molecular bands are evident in the remaining 38 objects (Mason et al. 2015), we restrict this discussion to the 12 galaxies with the highest quality data.

It is important to realize that these are not necessarily the galaxies where features due to TP-AGB stars would be expected to be the strongest. That is, no selection due to stellar population properties was made. The galaxies are simply those in which the data permit a close examination of the various bands that have been suggested to be signatures of TP-AGB stars. As shown in Table 1, with the exception of NGC 2832 and NGC 2768, all of the galaxies are spirals. Optical stellar population studies have been carried out for several of the galaxies, and in most cases old ages are suggested (Table 1). Possible exceptions are NGC 2655, NGC 2768 and NGC 5005. The H β line index in NGC2655 suggests a mean age of ∼2 Gyr (Sil'chenko 2006), while studies disagree about whether old (Sil'chenko 2006; Zhang, Gu & Ho 2008) or intermediate-age (Crocker et al. 2008; Serra et al. 2008) stars dominate in NGC 2768. In NGC 5005, Cid Fernandes et al. (2004a) find that an intermediate-age stellar population contributes about 45 per cent of the nuclear optical light.

Intercomparing stellar ages obtained from different spectral regions, apertures and line indices/stellar population models can be highly problematic. None the less we use this information in Section 4, in which we draw some tentative conclusions about the type of stars causing the molecular absorption features observed in this galaxy sample.

2.2 The data

The spectra were obtained using GNIRS' cross-dispersed mode, which provides simultaneous spectral coverage from ∼0.8 to 2.5 μm. The 0.3 arcsec slit was used, providing $R \sim 1200$, and was orientated at the mean parallactic angle at the time of the observations. The observations were executed in queue mode (Programs GN-2012B-Q-80, GN-2013A-Q-16), and the observing condition criteria allowed for observations to be taken with thin cirrus and seeing $\lesssim$1 arcsec. The data were reduced using standard procedures, described in Mason et al. (2015).

Some stellar features of interest are located in regions of poor atmospheric transmission, in which the telluric cancellation process (dividing by a slightly shifted and scaled spectrum of an A star observed near in time and airmass) may leave artefacts in the spectrum. For instance, the 0.93 μm feature lies close to telluric H_2O absorption at ∼0.95 μm. The authenticity of this feature was verified in two ways. First, the shifting and scaling applied to the standard star were adjusted, while verifying that the strength and profile of the feature were not significantly affected. Secondly, a standard star spectrum was reduced using the same procedure applied to the galaxies, showing that no similar feature was produced in the resulting spectrum (Fig. 1). A similar procedure was applied to the H_2O absorption regions, indicating that the broad H_2O bands apparent in some objects are not artefacts of the data reduction but true stellar features.

3 RESULTS

3.1 The spectral features

The full set of spectra is shown in Fig. 1, while Figs 2–4 show close-ups of various regions of interest. As can be seen from these figures (see also Fig. 6), the CN (1.1 μm, 1.4 μm) and CO (1.6 μm, 2.3 μm) bands are clearly detected in the majority of sources. While the 1.1 μm CN band is known in a number of galaxies (Riffel et al. 2007), the CN band at 1.4 μm has to date only been detected in NGC 4102 (Martins et al. 2013a). The CN 1.4 μm band falls in a region of poor atmospheric transmission and is therefore difficult to detect in low-redshift extragalactic sources. Thanks to the dry conditions under which these data were obtained; however, we detect the 1.4 μm CN band in almost all the galaxies of the present sample. According to M05, these bands are strong in TP-AGB stars, whose contribution to the integrated light peaks at intermediate ages.

The H_2O 1.4 μm band is also detected in almost all sources, while the 1.8 μm band is visible only in some (NGC 2655, NGC 2768, NGC 3147, NGC 4548, NGC 5850). C_2 lines are weak or absent in the individual galaxy spectra but the 1.76 μm band may show up in the mean spectrum (see Fig. 5). These features are present in the IRTF atlas of cool stars (see figs 7–34 of Rayner, Cushing & Vacca 2009, see also Cushing, Rayner & Vacca 2005), and are also predicted by M05 (their figs 14 and 15).

A comparison of the GNIRS spectra with the IRTF library shows that, besides the bands predicted by the M05 models, we also detect a VO feature at 1.048 μm. A comparison of our Fig. 1 with fig. 8 of Rayner et al. (2009) shows that the VO band at 1.048 μm, detected in many of the galaxies in our sample, most likely originate in late M III stars in the TP-AGB phase. To our knowledge, this is the first time that these bands have been reported in galaxies. A broad feature ranging between ∼0.93 and 0.95 μm is also detected, but the identity of the carrier is uncertain. The feature may be due to a combination of CN (red system, $\Delta v = v'' - v' = -1$), TiO (ϵ system, $\Delta v = -1$) and ZrO, which are all strong in the spectra of cool giant stars (Rayner et al. 2009). The 0.886 μm band due to the δ system of TiO ($\Delta v = 0$) is detected in some of the spectra (NGC 2832, NGC 4594 and perhaps others). Depending on the spectral coverage, the 0.843 μm $\Delta v = 0$ bandheads of the ϵ system of TiO are also detected in those objects, blended with the well-known Calcium triplet lines.

We have measured the equivalent widths (EW) of the strongest molecular bands, including the 0.93 μm CN/TiO/ZrO and 1.048 μm VO bands that are particularly relevant to TP-AGB stars. The measurements were performed using an updated version of the PACCE code (Riffel & Vale 2011). In this code, the continuum uncertainty is taken as the root mean square of the difference between the linear fit to the pseudo-continuum and the observed one. Then a Gaussian distribution of errors, using the above difference as 1σ standard deviation, is assumed to simulate new pseudo-continua. Finally, EW uncertainties are assumed to be the standard deviation of 500 measurements of EW using the simulated pseudo-continua as continuum points for the linear fit. The line definitions used are listed in Table 2 and the measured values are in Table 3.

As the spectra of the 12 galaxies have rather similar continuum and emission line properties (see Fig. 1), we averaged them to construct a spectrum with very high S/N, allowing further verification that the detected features are real. The spectra were normalized to unity at 1.223 μm before computing the mean value of the fluxes, pixel by pixel. The resulting spectrum (Fig. 5) supports the conclusion that the features observed in the individual galaxies are real,

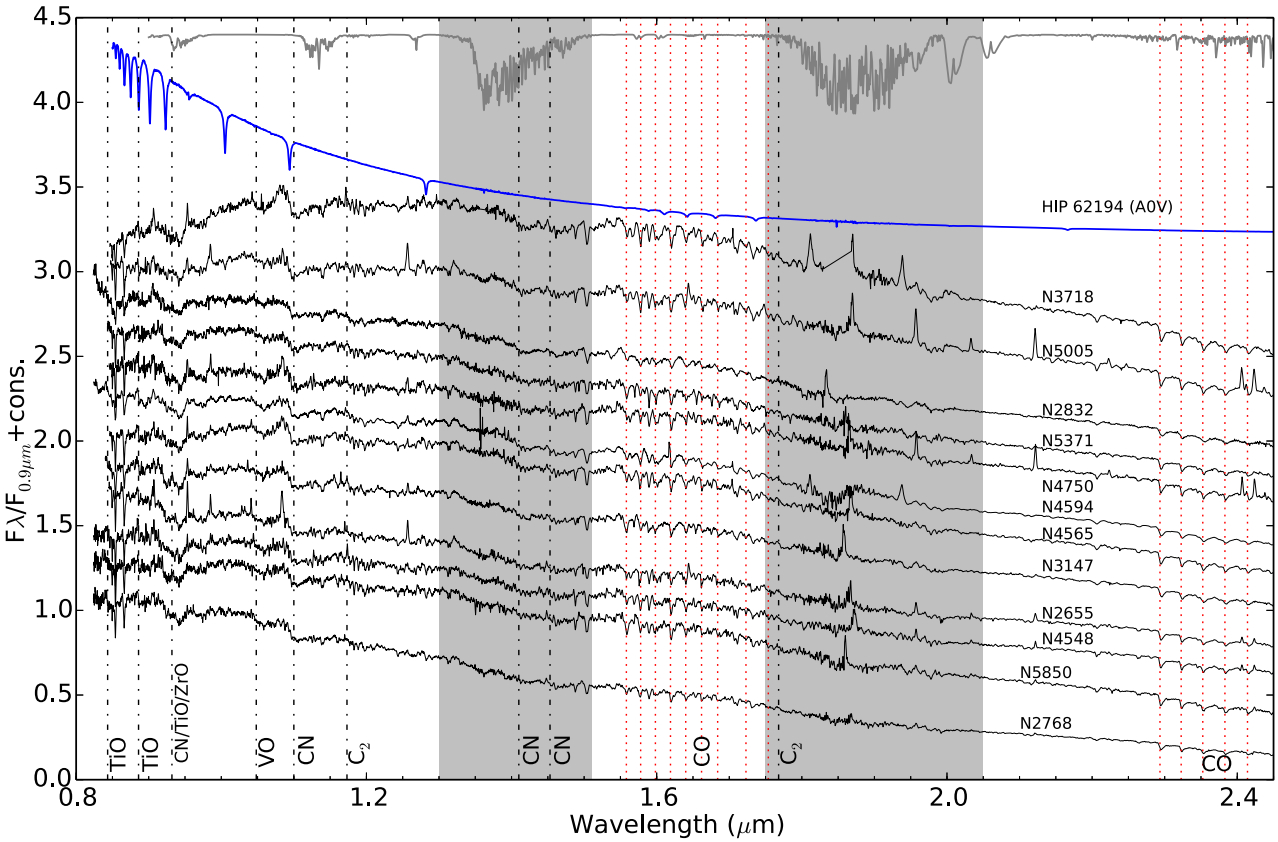

Figure 1. Rest frame spectra of the galaxy sample. Shaded regions indicate broad, stellar H_2O molecular bands, while dotted lines denote the CO bands. Other molecular bands are labelled at the bottom of the figure. A Mauna Kea atmospheric transmission spectrum for 1 mm H_2O and 1 airmass is also shown (grey), along with the spectrum of an A0 star (blue) reduced in the same manner as the galaxy data. Because of the small redshifts of the galaxies, the telluric features/residuals in the A0 star and atmospheric spectra do not correspond precisely to those in the galaxy data.

since they clearly appear in the mean spectrum. As the galaxies are at different redshifts, when they are shifted to the rest frame to create the mean spectrum, any systematic effects are shifted to different positions and will therefore tend to cancel out or be weakened in the mean spectrum. Additionally, (i) reducing a standard star using the same procedures results in a very clean spectrum with few weak telluric line residuals (Section 2), and (ii) we can fit the observed mean absorption spectrum very well using the IRTF stellar library (Section 4), thus indicating that the features are real and due to stars.

3.2 Stellar population synthesis

Bands from carbon-containing molecules are present in the galaxy spectra in Fig. 1, along with VO and possibly a contribution from ZrO in the band at 0.93 μm. The presence of these molecules suggests a significant contribution from TP-AGB stars to the NIR spectra of the galaxies. To further investigate (1) whether these molecular bands really are due to TP-AGB stars, and (2) whether the available stellar population synthesis models are able to reproduce them, we carry out a stellar population synthesis on the mean spectrum using the STARLIGHT spectral synthesis code (Cid Fernandes et al. 2004a, 2005a,b; Asari et al. 2007). The procedures followed are described in Riffel et al. (2009) and Dametto et al. (2014), including, for example, the methods used to handle extinction, emission lines and differences in spectral resolution. Briefly, STARLIGHT fits an observed spectrum O_λ with a combination, in different proportions, of N_* SSPs, solving the equation:

$$M_\lambda = M_{\lambda 0}\left[\sum_{j=1}^{N_*} x_j\, b_{j,\lambda}\, r_\lambda\right] \otimes G(v_*, \sigma_*), \quad (1)$$

where M_λ is a model spectrum, $b_{j,\lambda}\, r_\lambda$ is the reddened spectrum of the jth SSP normalized at λ_0; $r_\lambda = 10^{-0.4(A_\lambda - A_{\lambda 0})}$ is the reddening term; $M_{\lambda 0}$ is the theoretical flux at the normalization wavelength; $\boldsymbol{x}$ is the population vector, and $G(v_*, \sigma_*)$ is the Gaussian distribution used to model the line-of-sight stellar motions, which is centred at velocity v_* with dispersion σ_*. The final fit is carried out searching for the minimum of the equation:

$$\chi^2 = \sum_\lambda [(O_\lambda - M_\lambda) w_\lambda]^2, \quad (2)$$

where emission lines and spurious features are masked out by fixing $w_\lambda = 0$. The quality of the fit is accessed by $\chi^2_{\rm Red}$ which is the χ^2 given by equation (2) divided by the number of points used in the fit and by adev $= |O_\lambda - M_\lambda|/O_\lambda$, which is the percentage mean deviation over all fitted pixels. For a detailed description of STARLIGHT, see its manual.[1] For applications in the optical, see Cid Fernandes et al. (2005b), and in the NIR see Riffel et al. (2009).

We use four different approaches to define the base set of spectra used by the code, as follows: (i) *stars approach*: a base composed

[1] http://astro.ufsc.br/starlight/

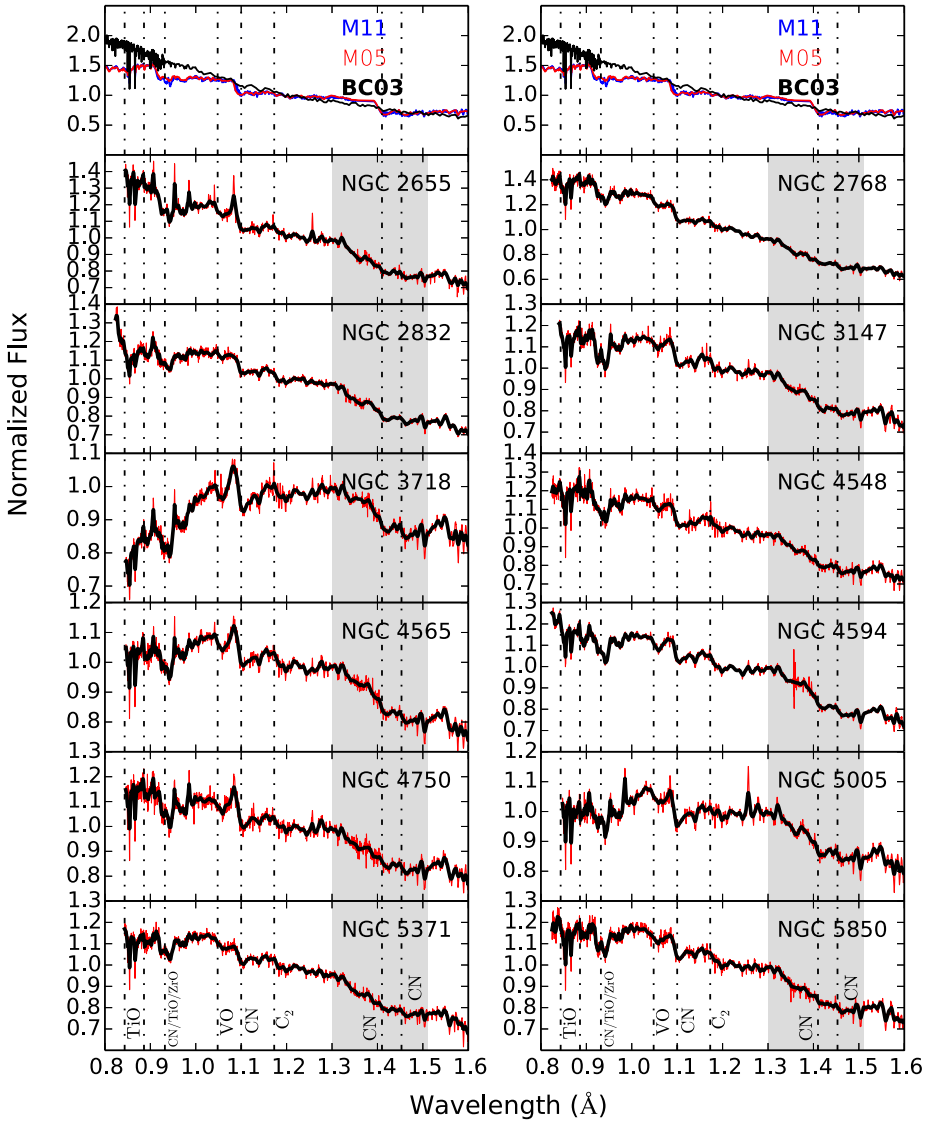

Figure 2. Close-up of the 0.8–1.6 μm region. Top: M11, M05 and BC03 models (Section 3.2). Other panels: observed spectrum (thin red line) and degraded to M05/BC03 spectral resolution (thick black line).

of all the 210 dereddened stars (spectral types F–S/C, F being the hottest available) in the IRTF spectral library (Cushing et al. 2005; Rayner et al. 2009) and (ii) *stars no TP-AGB approach*: the same as in (i) but removing all the TP-AGB stars from the base. (iii) *M11 approach*: EPS models of M11 (an example of models including empirical spectra of C- and O-rich TP-AGB stars), which consist of theoretical SSPs covering 12 ages ($t = 0.01$,0.03, 0.05, 0.1, 0.3, 0.5, 0.7, 1, 2, 5, 9 and 13 Gyr) at solar metallicity; (iv) *BC03 approach*: SSPs from BC03 (an example of models calibrated with broad-band photometry) with the same ages and metallicity as above.

4 DISCUSSION

4.1 Origin of the features

To link the molecular absorption features to the kind of star in which they may arise, we first revisit some relevant aspects of the later stages of stellar evolution.

Once the helium in the core of a star is exhausted, He burning begins in a shell surrounding the core. This marks the arrival of the star on the AGB. The star starts to expand, becoming cool and luminous, and develops a growing convective outer region. At this stage, the second dredge-up occurs, mixing the end points of helium burning, mainly C and O, into the star's atmosphere. At the end of this phase, the s process becomes the dominant mechanism of nuclear fusion, producing elements such as Zr and V (Habing & Olofsson 2004).

The star then starts to undergo thermal pulses, leaving the E-AGB stage and entering the TP-AGB phase. The third dredge-up takes place, and processed material from the star's interior is transported into its atmosphere. At this point the spectrum of the star will present evidence of enhanced C and O abundance, along with features due to species containing the newly formed Zr and V (Habing & Olofsson 2004). For example, the NIR CN absorption band is particularly enhanced in carbon stars, where there is residual carbon that is not bound with oxygen in CO molecules. As N-type carbon stars are produced after the third convective dredge-up along the TP-AGB

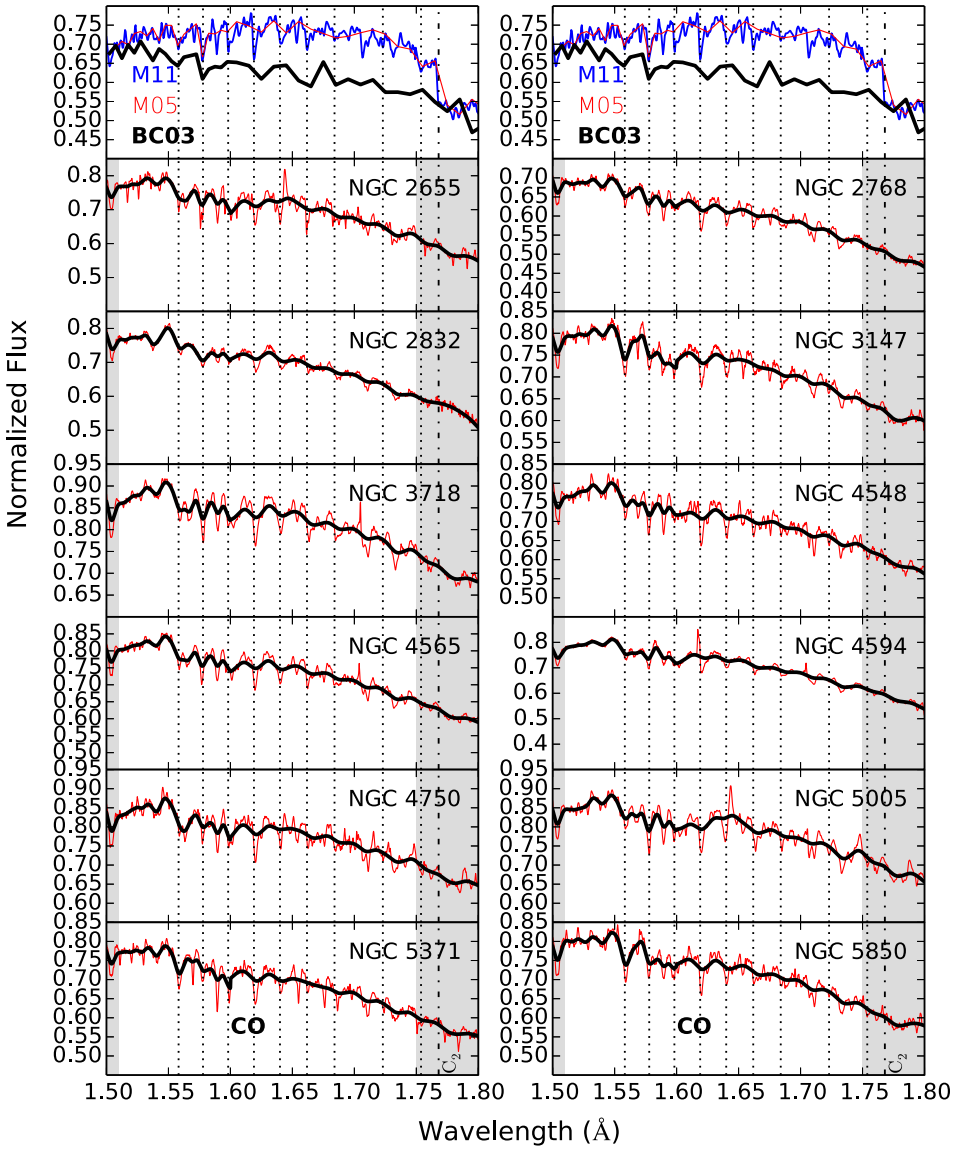

Figure 3. Same as Fig. 2.

phase (Habing & Olofsson 2004), the detection of deep CN features may indicate stellar populations rich in this kind of star (Lançon et al. 2001; Riffel et al. 2007). Similarly, VO and ZrO are produced with the residual oxygen not used in the formation of CO and TiO. Since V and Zr are only produced by the s process, these features are normally only detected in TP-AGB stars.

Below, we relate the spectral features in the galaxies to those observed in various kinds of star. It is therefore necessary to understand the stellar characteristics (spectral types and other traits) that identify a star as being in the TP-AGB phase. Most AGB stars have spectral classes M, S and C (Habing & Olofsson 2004). Of the two main types of carbon star, C-N stars are in the TP-AGB phase while C-R stars are not. All the molecular bands in C stars are from carbon-containing molecules. The spectra of early M-type stars contain TiO bands, while VO becomes apparent at later spectral types. S stars, however, are characterized by distinctive ZrO absorption. As noted above, s-process elements such as Zr and V are normally only present in AGB stars in the TP stage.

TP-AGB stars can also be distinguished by the variability caused by their long-period pulsations. The stellar library of Rayner et al. (2009) includes several IR spectra of TP-AGB stars, identified by their characteristic variability types (irregular, semi-regular and Mira), and their data illustrate the above trends. Inspecting their series of dwarf, giant and supergiant spectra (their figs 7–9) shows that the only molecular features detected in the dwarf stars are TiO, CO, H_2O and FeH. CN bands are present in the giants and supergiants, but are most prominent in the late-type supergiants with TP-AGB-like variability characteristics (the K1 Ia-Iab, K5 Ib, M3 Iab-Ia and M5 Ib-II stars in their fig. 9). ZrO also becomes prominent in the coolest of the TP-AGB supergiants in that figure. In the latest type of the TP-AGB giants (M4 III, M6 III, M7 III and M8-9 III in fig. 8 of Rayner et al. 2009), absorption from the VO molecule becomes apparent.

The results of the stellar population synthesis are shown in Fig. 5. When using the *stars approach* the spectrum can be well reproduced, and a significant fraction ($\sim$ 35 per cent) of the light comes from TP-AGB stars (the stars marked with $\star$ in the lower left panel

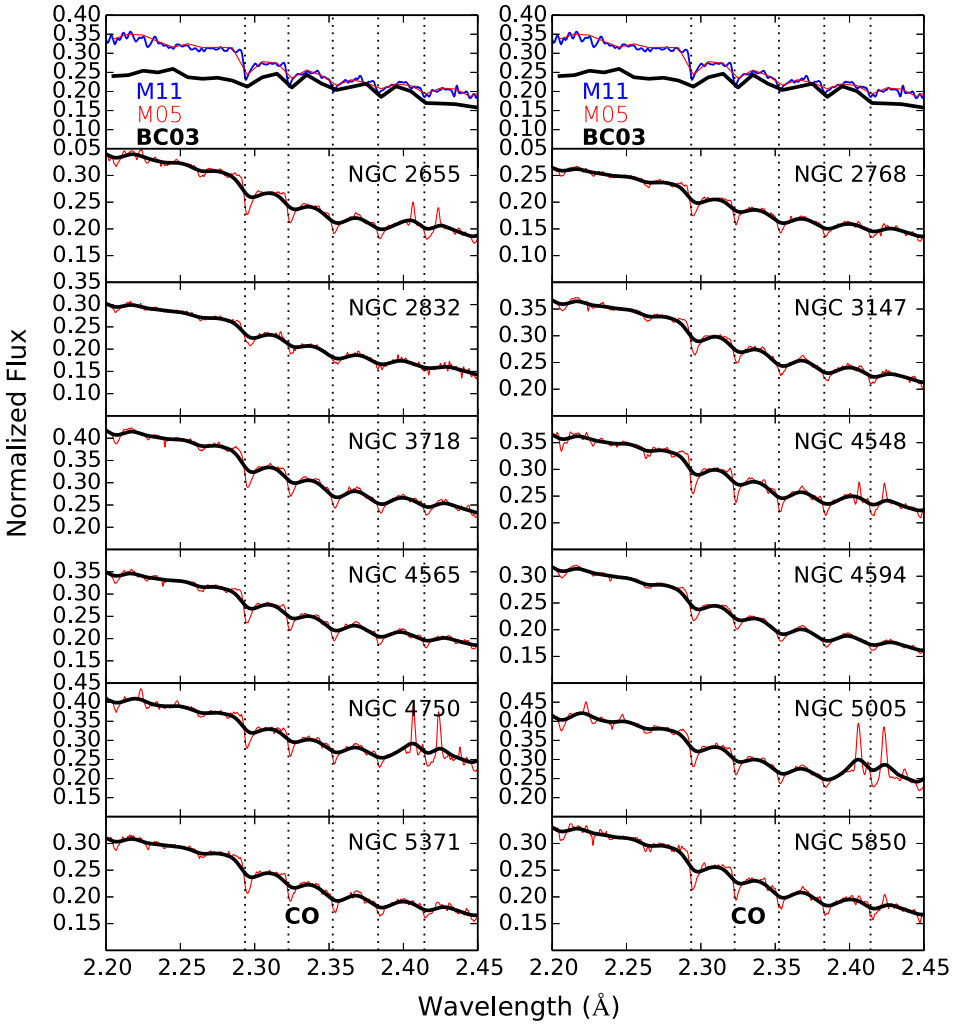

Figure 4. Same as Fig. 2.

of the figure). This is illustrated by Fig. 6, which shows that these stars account for the molecular features particularly at the short wavelength end of the spectrum. However, when the TP-AGB stars are removed, the code replaces them with a variety of E-AGB and red giant stars, notably a large contribution from a K5Ib star and a significant contribution from a C-R type carbon star. The quality of the fit is similar overall, with just a small increase in the χ^2 and $Adev^2$ values.

Taken at face value, this would suggest a degeneracy between R-type carbon-rich stars summed with E-AGB stars and the TP-AGB stars. However, there are two important details that have to be taken into account. First, we are trying to fit a galaxy's stellar population with the observed spectra of stars from a library which is neither complete nor absolutely flux-calibrated, and most importantly, not constrained by the rules of stellar evolution, which would require the use of an isochrone and an assumption about the initial mass function. This would be the correct approach to create an SSP,[3] where the contribution of each stellar spectral type is weighted by the number and luminosity of the stars. This is a large task in its own right and is well beyond the scope of this paper. This means that although we can reproduce the mean spectrum with both approaches, the results need to be taken with caution. AGB and regular giant stars are short-lived, and their true contribution to a stellar population spectrum of a given age cannot be determined by the approaches we described here.

With that said, TP-AGB stars are very luminous. Despite the fact that they exist only in population components with ages ∼0.2–2 Gyr (M05), they have been shown to account for almost 20 per cent of the 1.6 μm flux of nearby galaxies (Melbourne et al. 2012), with much of the remainder likely coming from relatively featureless main-sequence stars. In the *K* band, they may be responsible for roughly half the total luminosity (Salaris et al. 2014). Such luminous stars, with strong absorption features, may be expected to leave an imprint on the NIR spectrum. Also, there is a subtle difference between the two fits in the absorption band at 0.93 μm (see Fig. 7). As noted above, this band probably contains contributions from CN, TiO and ZrO. The fit in this region is improved when TP-AGB stars are included, suggesting that some of the absorption indeed comes from the Zr brought to the surface by the third dredge-up. Combined with the fact that VO is present in the galaxies'

[2] The percentage mean $|O_\lambda - M_\lambda|/O_\lambda$ deviation over all fitted pixels.
[3] Which are the correct inputs for the base of elements in stellar population fitting using the STARLIGHT code.

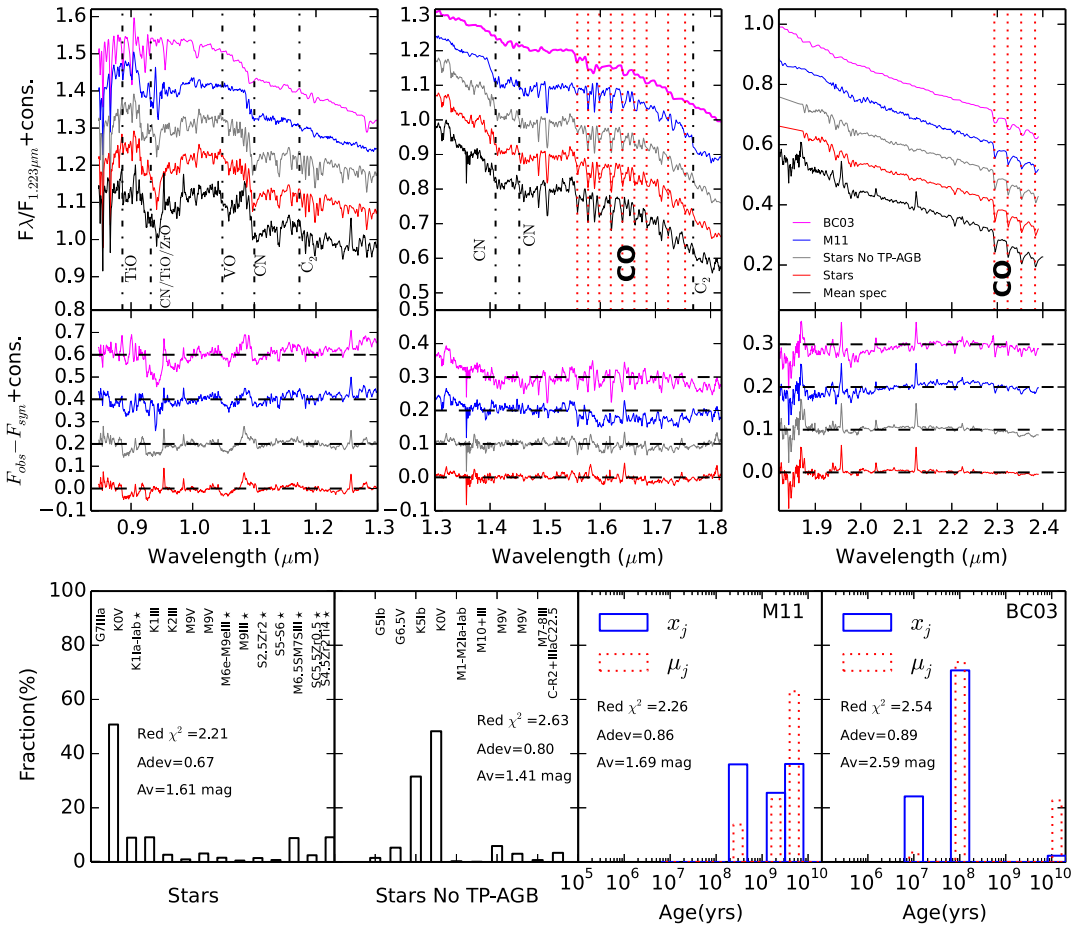

Figure 5. Top: mean spectrum (black), along with EPS fits using (lowest to highest) the IRTF stars, stars no TP-AGB, M11 and BC03 models. Middle: the difference between the mean spectrum and its fits, following the same order as in the top. Bottom: synthesis results from these three methods. x_j denotes light fractions and μ_j denotes mass fractions. Stars spectral types are taken from Cushing et al. (2005) and Rayner et al. (2009) and ⋆ denotes TP-AGB stars. The goodness of the fits and *Av* are on the labels. For display purposes, we removed from the histograms stars in the base set that do not contribute to the fits.

Table 2. Line limits and continuum bandpasses.

ID	Line limits (μm)	Continuum bandpass (μm)
CN/TiO/ZrO	0.9200–0.9500	0.8760–0.8800, 0.9570–0.9650
VO	1.0470–1.0650	1.0350–10 390, 1.0660–1.0740
CN11 (α)	1.0900–1.1300	1.0660–10 740,1.1310–1.1360
CN14a	1.4050–1.4300	1.3950–13 990, 1.4340–1.4390, 1.4750–1.4840
CN14b	1.4500–1.4715	1.3950–13 990, 1.4340–1.4390, 1.4750–1.4840
CO16a	1.5735–1.5810	1.5110–15 170, 1.5390–1.5410, 1.6270–1.6310, 1.6570–1.6580
CO16b(α)	1.6175–1.6285	1.5110–15 170, 1.5390–1.5410, 1.6270–1.6310, 1.6570–1.6580
CO22a(α)	2.2910–2.3200	2.2690–22 790, 2.3950–2.3999
CO22b(α)	2.3200–2.3420	2.2690–227 90, 2.3950–2.3999
CO22c(α)	2.3420–2.3695	2.2690–227 90, 2.3950–2.3999

Notes. α based on Riffel et al. (2009) and Riffel et al. (2011a).

spectra (see Fig. 6), these considerations suggest that TP-AGB stars play a significant role in the features observed in our integrated spectra.[4]

If TP-AGB stars dominate the NIR spectral features, we might expect to observe stronger features in intermediate-age galaxies

[4] We note that the VO feature near 1.05 μm is not well reproduced by either the models or the stellar library. The absence of the feature in the model spectra is not surprising, as they do not include the VO molecule. Its weakness in the empirical fit may be a result of incompleteness of the stellar library or the fact we are not constraining it by the rules of stellar evolution. A definite conclusion will require more detailed analysis, and is left for a future paper (Riffel et al., in preparation)

Table 3. EWs of the absorption bands in the galaxy sample.

Galaxy	CN/TiO/ZrO	VO	CN11	CN14a	CN14b	CO16a	CO16b	CO23a	CO23b	CO23c
NGC 2655	20.20 ± 0.50	3.66 ± 0.37	12.06 ± 0.52	8.31 ± 0.50	4.71 ± 0.34	4.12 ± 0.13	6.84 ± 0.19	23.31 ± 0.24	22.60 ± 0.30	29.83 ± 0.42
NGC 2768	17.23 ± 0.53	3.75 ± 0.24	11.14 ± 0.46	5.09 ± 0.58	5.88 ± 0.37	3.23 ± 0.07	6.45 ± 0.11	23.97 ± 0.27	22.61 ± 0.22	30.42 ± 0.33
NGC 2832	16.16 ± 0.49	2.17 ± 0.35	11.24 ± 0.51	8.88 ± 0.34	5.00 ± 0.27	4.30 ± 0.10	4.85 ± 0.27	21.59 ± 0.43	21.24 ± 0.43	30.63 ± 0.68
NGC 3147	23.80 ± 0.41	3.23 ± 0.46	9.45 ± 0.51	6.68 ± 0.42	3.62 ± 0.38	2.39 ± 0.08	5.87 ± 0.16	18.92 ± 0.21	17.44 ± 0.29	24.18 ± 0.40
NGC 3718	18.34 ± 0.58	4.92 ± 0.32	9.07 ± 0.61	8.22 ± 0.49	4.92 ± 0.39	3.37 ± 0.09	6.28 ± 0.19	22.36 ± 0.33	20.58 ± 0.26	27.90 ± 0.37
NGC 4548	22.58 ± 0.75	3.94 ± 0.45	10.49 ± 1.15	6.33 ± 0.70	4.74 ± 0.47	3.33 ± 0.10	6.90 ± 0.17	20.33 ± 0.25	18.77 ± 0.25	25.97 ± 0.36
NGC 4565	16.61 ± 0.44	3.43 ± 0.24	9.01 ± 0.49	7.63 ± 0.49	4.16 ± 0.31	3.64 ± 0.08	6.66 ± 0.17	21.98 ± 0.25	20.94 ± 0.24	28.45 ± 0.42
NGC 4594	20.07 ± 0.40	4.81 ± 0.24	8.07 ± 0.40	10.43 ± 1.02	3.74 ± 0.37	3.41 ± 0.07	3.68 ± 0.16	23.80 ± 0.16	22.13 ± 0.16	30.86 ± 0.32
NGC 4750	16.44 ± 0.61	3.98 ± 0.40	8.32 ± 0.56	5.37 ± 0.55	4.43 ± 0.33	1.96 ± 0.08	6.41 ± 0.15	20.86 ± 0.28	20.61 ± 0.30	26.45 ± 0.48
NGC 5005	11.86 ± 0.41	1.70 ± 0.32	10.52 ± 0.53	7.93 ± 0.23	3.39 ± 0.27	4.28 ± 0.08	6.15 ± 0.13	22.80 ± 0.22	23.16 ± 0.26	30.06 ± 0.48
NGC 5371	16.80 ± 0.48	1.75 ± 0.34	7.26 ± 0.67	4.84 ± 0.38	3.81 ± 0.35	1.94 ± 0.12	6.41 ± 0.21	22.65 ± 0.25	20.62 ± 0.28	28.82 ± 0.44
NGC 5850	18.45 ± 0.51	3.11 ± 0.39	10.06 ± 0.66	3.85 ± 0.44	3.87 ± 0.31	3.07 ± 0.09	6.72 ± 0.14	22.58 ± 0.30	21.94 ± 0.26	29.15 ± 0.34

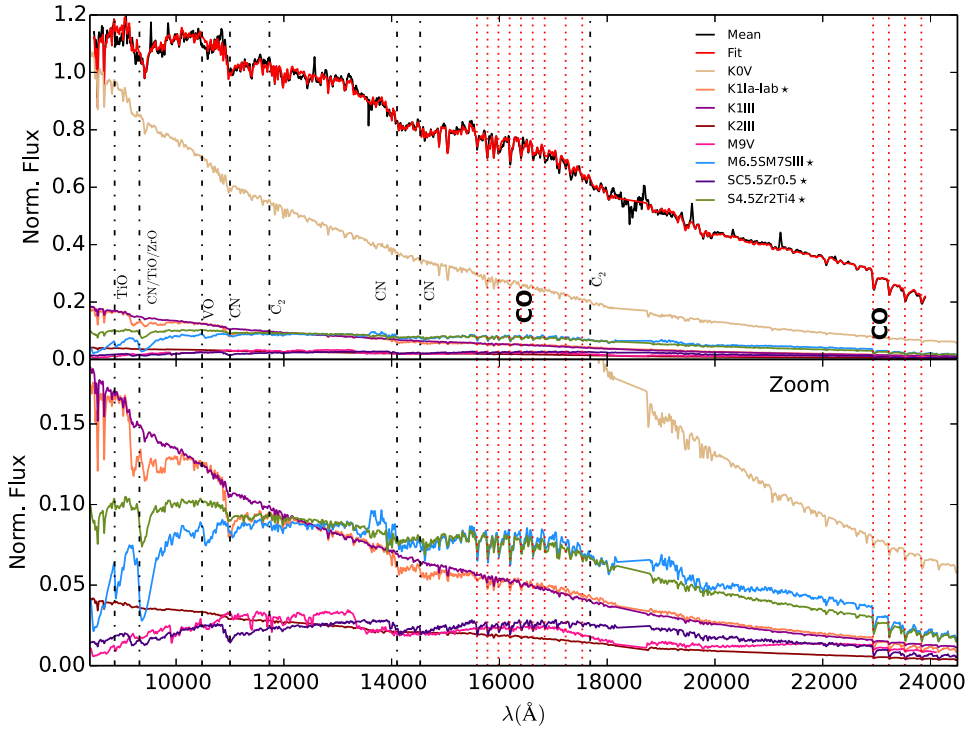

Figure 6. Fractional contribution of the stars used in the fit using the stars approach (Top). For display purposes, we removed the stars contributing with less than 2 per cent (to see the contribution of stars contributing with less than 2 per cent see Fig. 5) from the plot. The contribution of the TP-AGB stars (marked with ⋆) to the observed absorption features is clearly observed, a zoom to these features is shown at the bottom. For more details, see Section 3.2.

that should host larger populations of these stars. This is not obviously the case in this sample. The spectra in Fig. 1 are remarkably similar, and there is no clear relationship between the EW values in Table 3 and whether a galaxy is classified as intermediate age or old in Table 1. Of the galaxies in this sample, NGC 5005 has probably the most secure evidence for a large intermediate-age (∼45 per cent) stellar population (Cid Fernandes et al. 2004b). Its CN/TiO/ZrO and VO bands, however, are the weakest that we observe (Table 3). Similarly, Mason et al. (2015) examined three galaxies with intermediate-age populations and found them to have weaker molecular absorption bands than older galaxies.

There are several possible reasons for this apparent contradiction. First, stellar populations derived from optical and NIR spectroscopy cannot necessarily be directly compared. Dust can obscure young populations in the optical, and different slit sizes[5] can probe different regions of spatially varied populations (Riffel et al. 2011b; Martins et al. 2013b). Secondly, the intermediate-age galaxies studied here and in Mason et al. (2015) likely span only limited range of metallicity. As the strength of TP-AGB spectral features depends greatly on their age and metallicity (M05), weak NIR features like those observed in NGC 5005 may not be a universal characteristic of intermediate-age galaxies. Thirdly, intermediate-age galaxies may also contain young stellar populations, whose relatively featureless spectra may dilute the stronger bands of the TP-AGB stars.

[5] That might be the case of NGC5005, since the slit used by Cid Fernandes et al. (2004b) is three times wider than ours, thus potentially sampling additional stellar populations.

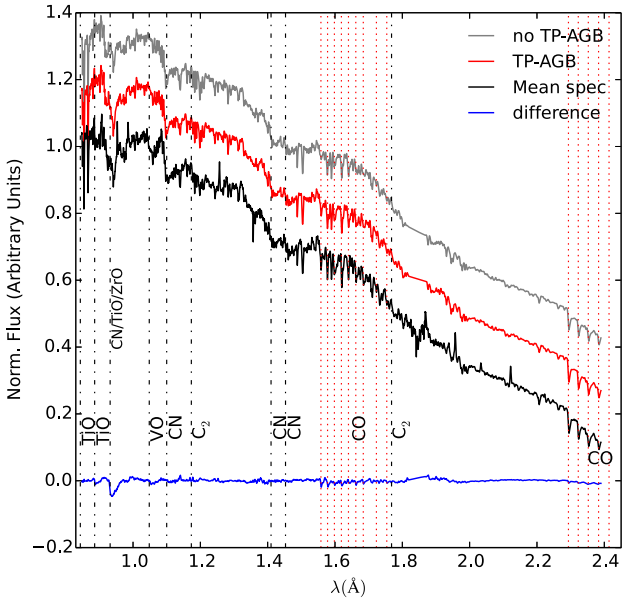

Figure 7. Difference between the stars and stars no-TP-AGB approaches presented in Fig. 5.

Finally, as shown by our model fits, red giants, C-R and E-AGB stars can also produce most of the observed features sometimes attributed to TP-AGB stars. These stars may be important in stellar populations that are both younger than the intermediate-age populations in which TP-AGB stars are believed to be abundant (if R C-rich and E-AGB stars are present in large fractions), or in older populations (which contain large numbers of red giants). This clearly demonstrates that to accurately model a stellar population, all kinds of evolved stars need to be taken into account.

To date, the most targeted search for TP-AGB stars in galaxies is that of Zibetti et al. (2013). They obtained NIR (*H*- and *K*-band) spectra of 16 post-starburst galaxies, selected partly for the CN (1.41 μm) and C_2 (1.77 μm) bands to be redshifted out of strong telluric absorption ($z \sim 0.2$). Although the stellar ages (0.5–1.5 Gyr) of these galaxies correspond to the period of maximum contribution of TP-AGB stars to the integrated spectrum, the depth of absorption features from carbon molecules in these stars was found to be no more than a few per cent of the continuum. Extrapolating from our observations to predict the features expected in post-starburst galaxies is beyond the scope of this paper, but we note that the weak CN and C_2 absorptions reported here would not be detected at the resolution (∼300 versus 1200) and S/N (∼30 versus 110 in the *K* band) of the Zibetti et al. (2013) data, and their spectral coverage does not include most of the other features that we report. It is therefore difficult to gauge whether our interpretation of the molecular features as dominated by TP-AGB stars is in conflict with the observations of Zibetti et al. (2013). However, it is clear that the features in the post-starburst galaxies are not as strong as predicted by the M05 models for galaxies of those ages and metallicities.

4.2 Performance of the models

The last two approaches tested in Section 3.2 (M11 approach and BC03 approach) are intended to show how well different SSP recipes are able to reproduce these features. Fitting the mean spectrum with the M11 models results in a complex star formation history, with similar fractions of young ($t < 1$ Gyr), intermediate-age ($t \sim 1$ Gyr) and old ($t \sim 10$ Gyr) SSPs. With the BC03 models, though, STARLIGHT includes a young ($\sim 10^7$ yr) component and requires only a very small fraction of old SSPs. This is probably because the BC03 models do not have deep NIR CN bands, causing the code to attempt to fit the 1.1 μm CN band with Pa γ. If such a young component were genuinely present, we would expect to require a significant fraction of F stars (the hottest available in the IRTF library) when fitting the mean spectrum with the stellar library, which is not the case. Furthermore, if we remove the ≤100 Myr components in the BC03 approach, the best fit is achieved with ∼35 per cent of the light due to the 1 Gyr and ∼65 per cent due to the 2 Gyr components, but with a much poorer fit ($\chi^2 \sim 100$).

The high (∼65 per cent) light fraction of stars with ages 0.2–3×10^9 yr in the M11 model fits ostensibly supports our previous interpretation that the molecular bands likely contain a strong contribution from TP-AGB stars, which should dominate the NIR emission of a stellar population of this age. However, this result could be coincidental: the M11 models include empirical spectra with good spectral resolution only for the TP-AGB stars, meaning only the intermediate-age stellar population in their models will present these features. As discussed above, most of the features can be reproduced with a mix of E-AGB and R C-rich stars, which means older stellar populations probably also have these features at some level. To avoid misinterpreting NIR galaxy spectra, it is thus of great importance to include high-quality empirical spectra of the other evolutionary phases in the EPS models.

While the M11 models qualitatively reproduce several of the broad absorption bands in the mean spectrum (notably CO and CN), these bands are weaker or absent in the BC03 model fit. This is probably not related to the different spectral resolution of the models ($R \sim 200$, versus $R \sim 500$ in M11) because we find that similar results are obtained from the M11 and M05 models (the latter with $R \sim 250$ in the *K* band). The differences are more likely related to uncertainties in the theoretical treatment of AGB and TP-AGB stellar phases and the fact that the M05/M11 models include empirical spectra of C and O-rich stars and therefore better account for these features.

Since the relative band strengths depend on metallicity (M05), we also tried fitting the mean spectrum with BC03 and M05 models including three non-solar metallicities (the M11 models include only solar metallicity for this wavelength range). Similar ages to those derived from the original analysis were obtained in all cases, and changing the metallicity did not significantly improve the fits to the features. This may suggest that the incompleteness in stellar types/phases of the empirical spectra on which the models are based is the first-order problem in reproducing the NIR absorption features. At this stage in the development of the models, metallicity probably plays a secondary role in predicting the strength of the features

5 FINAL REMARKS

We have presented high S/N, 0.85–2.5 μm spectra of the nuclei of 12 local galaxies. The spectra show indications of numerous weak molecular absorption bands that arise in the atmospheres of cool stars. While several types of evolved stars can exhibit most of the detected features, we argue that the high luminosity of TP-AGB stars, and the fact that the spectra contain VO and likely ZrO, that are only expected in stars undergoing thermal pulses, imply that these features are the long-debated signatures of TP-AGB stars. However, a combination of R-type carbon-rich stars and E-AGB

stars should not be ruled out as an important contributor to these bands.

In testing, two sets of stellar population synthesis models against these spectra, we found that models that include stars with relatively strong absorption bands provide a more accurate representation of the spectra. However, to avoid misinterpreting the data, future models must include high-quality spectra of C-R and E-AGB stars, along with those of TP-AGB stars. Testing the predictions of EPS models has to date been hampered by a lack of high-quality data against which the models can be tested, and we hope that the high S/N and wavelength coverage of the spectra presented here will make them a useful aid to the development of such models. The reduced spectra presented here are available at: http://www.canfar.phys.uvic.ca/vosui/#/karun/xdgnirs_Dec2014/XD_final.

ACKNOWLEDGEMENTS

We thank the anonymous referee for useful comments. The Brazilian authors thank CNPq and FAPERGS support. RR acknowledges M. Cushing, L. Girardi, C. Maraston, A. Romero and R. P. Schiavon for helpful discussions as well as CNPq and FAPERGS for financial support. LCH acknowledges support by the Chinese Academy of Science through grant no. XDB09030102 (Emergence of Cosmological Structures) from the Strategic Priority Research Program and by the National Natural Science Foundation of China through grant No. 11473002. CRA is supported by a Marie Curie Intra European Fellowship within the 7th European Community Framework Programme (PIEF-GA-2012-327934). Based on observations obtained at the Gemini Observatory, operated by the Association of Universities for Research in Astronomy, Inc., under a cooperative agreement with the NSF on behalf of the Gemini partnership: the National Science Foundation (US), the Science and Technology Facilities Council (UK), the National Research Council (Canada), CONICYT (Chile), the Australian Research Council (Australia), Ministério da Ciência e Tecnologia (Brazil) and Ministerio de Ciencia, Tecnología e Innovación Productiva (Argentina).

REFERENCES

Asari N. V., Cid Fernandes R., Stasińska G., Torres-Papaqui J. P., Mateus A., Sodré L., Schoenell W., Gomes J. M., 2007, MNRAS, 381, 263
Bruzual G., Charlot S., 2003, MNRAS, 344, 1000 (BC03)
Cid Fernandes R., Gu Q., Melnick J., Terlevich E., Terlevich R., Kunth D., Rodrigues Lacerda R., Joguet B., 2004a, MNRAS, 355, 273
Cid Fernandes R. et al., 2004b, ApJ, 605, 105
Cid Fernandes R., González Delgado R. M., Storchi-Bergmann T., Martins L. P., Schmitt H., 2005a, MNRAS, 356, 270
Cid Fernandes R., Mateus A., Sodré L., Stasińska G., Gomes J. M., 2005b, MNRAS, 358, 363
Conroy C., 2013, ARA&A, 51, 393
Conroy C., Gunn J. E., 2010, ApJ, 712, 833
Crocker A. F., Bureau M., Young L. M., Combes F., 2008, MNRAS, 386, 1811
Cushing M. C., Rayner J. T., Vacca W. D., 2005, ApJ, 623, 1115
Dametto N. Z., Riffel R., Pastoriza M. G., Rodríguez-Ardila A., Hernandez-Jimenez J. A., Carvalho E. A., 2014, MNRAS, 443, 1754
de Lorenzo-Cáceres A., Falcón-Barroso J., Vazdekis A., 2013, MNRAS, 431, 2397
Dottori H., Díaz R. J., Carranza G., Lípari S., Santos J., Jr, 2005, ApJ, 628, L85
Elias J. H., Joyce R. R., Liang M., Muller G. P., Hileman E. A., George J. R., 2006, Proc. SPIE, 6269, 62694C
Habing H. J., Olofsson H., 2004, Asymptotic Giant Branch Stars. Springer-Verlag, Berlin
Ho L. C., Filippenko A. V., Sargent W. L., 1995, ApJS, 98, 477
Ho L. C., Filippenko A. V., Sargent W. L. W., 1997, ApJS, 112, 31
Kriek M. et al., 2010, ApJ, 722, L64
Lançon A., Goldader J. D., Leitherer C., González Delgado R. M., 2001, ApJ, 552, 150
Loubser S. I., Sánchez-Blázquez P., Sansom A. E., Soechting I. K., 2009, MNRAS, 398, 133
Lyubenova M., Kuntschner H., Rejkuba M., Silva D. R., Kissler-Patig M., Tacconi-Garman L. E., Larsen S. S., 2010, A&A, 510, A19
Lyubenova M., Kuntschner H., Rejkuba M., Silva D. R., Kissler-Patig M., Tacconi-Garman L. E., 2012, A&A, 543, A75
Maraston C., 2005, MNRAS, 362, 799 (M05)
Maraston C., Strömbäck G., 2011, MNRAS, 418, 2785 (M11)
Maraston C., Daddi E., Renzini A., Cimatti A., Dickinson M., Papovich C., Pasquali A., Pirzkal N., 2006, ApJ, 652, 85
Marigo P., 2014, preprint (arXiv:1411.3126)
Marigo P., Girardi L., Bressan A., Groenewegen M. A. T., Silva L., Granato G. L., 2008, A&AS, 482, 883
Martins L. P., Rodríguez-Ardila A., Diniz S., Gruenwald R., de Souza R., 2013a, MNRAS, 431, 1823
Martins L. P., Rodríguez-Ardila A., Diniz S., Riffel R., de Souza R., 2013b, MNRAS, 435, 2861
Mason R. E. et al., 2015, ApJS, 217, 13
Melbourne J. et al., 2012, ApJ, 748, 47
Mouhcine M., Lançon A., 2002, A&A, 393, 149
Noël N. E. D., Greggio L., Renzini A., Carollo C. M., Maraston C., 2013, ApJ, 772, 58
Ramos Almeida C., Pérez García A. M., Acosta-Pulido J. A., 2009, ApJ, 694, 1379
Rayner J. T., Cushing M. C., Vacca W. D., 2009, ApJS, 185, 289
Riffel R., Vale T. B., 2011, Ap&SS, 334, 351
Riffel R., Pastoriza M. G., Rodríguez-Ardila A., Maraston C., 2007, ApJ, 659, L103
Riffel R., Pastoriza M. G., Rodríguez-Ardila A., Bonatto C., 2009, MNRAS, 400, 273
Riffel R., Ruschel-Dutra D., Pastoriza M. G., Rodríguez-Ardila A., Santos J. F. C., Jr, Bonatto C. J., Ducati J. R., 2011a, MNRAS, 410, 2714
Riffel R., Bonatto C., Cid Fernandes R., Pastoriza M. G., Balbinot E., 2011b, MNRAS, 411, 1897
Salaris M., Weiss A., Cassarà L. P., Piovan L., Chiosi C., 2014, A&A, 565
Sánchez-Blázquez P., Gorgas J., Cardiel N., González J. J., 2006, A&A, 457, 809
Sarzi M., Rix H.-W., Shields J. C., Ho L. C., Barth A. J., Rudnick G., Filippenko A. V., Sargent W. L. W., 2005, ApJ, 628, 169
Serra P., Trager S. C., Oosterloo T. A., Morganti R., 2008, A&A, 483, 57
Sil'chenko O. K., 2006, ApJ, 641, 229
Zhang Y., Gu Q.-S., Ho L. C., 2008, A&A, 487, 177
Zibetti S., Gallazzi A., Charlot S., Pierini D., Pasquali A., 2013, MNRAS, 428, 1479

This paper has been typeset from a TEX/LATEX file prepared by the author.